PCCP

Accepted Manuscript

ROYAL SOCIETY OF CHEMISTRY

www.rsc.org/pccp

Journal Name

RSCPublishing

ARTICLE

Synthesis and luminescent properties of $La_{1-x}Nd_xP_5O_{14}$ nanocrystals

Cite this: DOI: 10.1039/x0xx00000x

Received 00th January 2012,
Accepted 00th January 2012

DOI: 10.1039/x0xx00000x

www.rsc.org/

L. Marciniak,[a*] W. Strek,[a] Y.Guyot[b] and D. Hreniak[a],

$La_{1-x}Nd_xP_5O_{14}$ nanocrystals were synthesized by coprecipitation method. Their structure and morphology were determined. The luminescence and excitation spectra of $La_{1-x}Nd_xP_5O_{14}$ nanocrystals were measured in the entire range of Nd^{3+} concentration. It was found that the relative intensities of absorption transitions increased significantly with concentration due to the cooperative interactions. The effect of concentration on fluorescence transitions was investigated. It was found the intensity of the $^4F_{3/2}\rightarrow{}^4I_{11/2}$ transition significantly increased with concentration relative to the resonant $^4F_{3/2}\rightarrow{}^4I_{9/2}$ transition almost three times due to strong reabsorption. The concentration quenching of fluorescence was discussed in terms of the Yokota-Tanimoto model.

Introduction

Lanthanides ultraphosphate (LnP_5O_{14}) belongs to the family of the so-called stoichiometric phosphors and the neodymium pentaphosphates NdP_5O_{14} crystals are the most known representatives due to their unique physical and chemical properties, such as good chemical and mechanical stability[1], relatively low thermal expansion coefficient[2-4] and efficient luminescence yield at high concentration Nd^{3+} ions. A predominant number of applications was based on interesting optical properties of NdP_5O_{14} crystals[1,5-13]. In this host lanthanide, ions are well separated from each other by the $(PO_3)^-$ tetrahedrons. The distance between optically active ions in the closest vicinity is relatively large (around 5.2 Å). Due to a long distance between the Nd^{3+} ions, the probability of a multipolar interaction between them is greatly reduced what entails lowered luminescence concentration quenching. Hence much attention has been paid to using neodymium ultraphosphates in laser technology[5-13]. First laser based on heavily Nd^{3+}-doped host was reported for a NdP_5O_{14} crystal[14] and was especially important from the laser miniaturization point of view. Concentration of dopants several dozen higher than in a case of YAG:1%Nd, with a relatively long lifetime (~ 120 μs) and strong luminescence intensity with unbroadened emission line are the key features of pentaphosphates. Moreover, a significantly lower threshold of the laser action reported for NdP_5O_{14} crystal around 0.45mW classifies those materials, together with $LiNdP_4O_{12}$ (threshold around 0.36mW), as one of the most important hosts for laser oscillation[5]. Crystals of neodymium pentaphosphates reveal tendency to twinning due to their ferroelastic properties, which becomes a problem for laser crystals preparation with reduced defects. Spectroscopic properties of neodymium phosphates crystals and glasses have been reported by many authors[15-22]. Recently we have reported on optical properties of $LiLa_{1-x}Nd_xP_4O_{12}$ nanocrystals[14,19-26] and $LiLa_{1-x}Dy_xP_4O_{12}$ nanocrystals[23]. In this paper we report synthesis, structural and spectroscopic properties of the $La_{1-x}Nd_xP_5O_{14}$ nanocrystals. Despite the fact that the spectroscopic properties and laser engineering of $La_{1-x}Nd_xP_5O_{14}$ crystals have been thoroughly investigated[1,5-13] no spectroscopic studies of respective nanocrystals have been performed. In particular our interest was focused on the concentration quenching of the Nd^{3+} luminescence and the mechanism of cooperative interactions.

Experimental

Nanocrystals of lanthanum pentaphosphates doped with neodymium ions ($La_{1-x}Nd_xP_5O_{14}$) were synthesized by a coprecipitation method. Lanthanum oxide (La_2O_3 99.99% from

Stanford Materials Corporation), neodymium oxide (Nd_2O_3 99.95% from Stanford Materials Corporation) and diammonium phosphate ($(NH_4)_2HPO_4$ from Sigma Aldrich) were used as starting materials. Appropriate amounts of lanthanum oxides were diluted in nitric acid in order to obtain nitrates. Afterwards, water solution of nitrates was combined with water solution of diammonium phosphates and the obtained solution was stirred using magnetic stirrer for 7 h and dried at 90°C for 48 h. Obtained precursor was grinded in a mechanical mill for 2 h in order to achieve homogenization followed by sintering for 6 h in 550°C.

The X-ray diffraction measurements (XRD) of $La_{1-x}Nd_xP_5O_{14}$ nanocrystalline powders were measured in Bragg-Brentano geometry on PANalytical X'Pert Pro diffractometer with a beta-filtered Cu Kalpha radiation (λ = 0.15418 nm). Transmission electron microscopy (TEM) images were taken with a JEM-2100F microscope under an operating voltage of 200 kV. The back scattering absorption spectra of nanocrystalline powders were measured using Varian Cary 5 UV-VIS Spectrophotometer.

The emission spectra were measured in the 800-1700 nm range with a CCD IDUS near-infrared InGaAs camera from ANDOR equipped with a 900 line/mm grating blazed at 1300 nm under 808 nm excitation line of a laser diode.

Decay profiles were measured using digital oscilloscope LeCroy WaveSurfer 400 and 532 nm excitation line of pulsed Nd:YAG (2^{nd} harmonic) and Horiba Jobin–Yvon HR1000 monochromator supplied with a Hamamatsu R5108 photomultiplier tube. Low temperature measurements were performed using a HC2 cryostat from APD Cryogenics equipped with a 330 Autotuning Temperature Controller from Lake Shore. The low temperature measurements were carried out in a closed flow cryostat.

Results and discussion

There are three types of crystallographic groups into which LnP_5O_{14} structure can crystallize: monoclinic P21/c, monoclinic C2/c and orthorombic Pncm[28-30]. However, at room temperature the monoclinic P21/c phase is dominant. The ferroelastic phase transition was observed at ~426 K[3]. The structure of NdP_5O_{14} is presented in Fig. 1a. One can notice characteristic ribbons of $(PO_4)^-$ tetrahedrons and well separated Nd^{3+} ions.

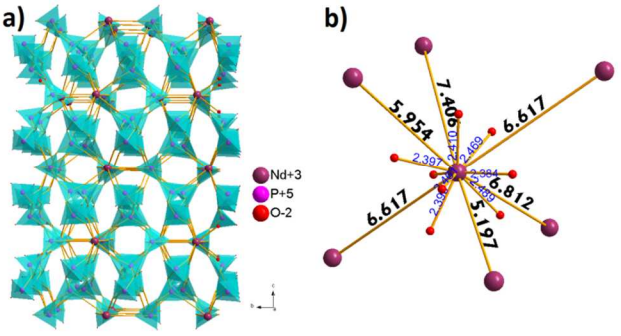

Figure 1. Structure visualization of a NdP_5O_{14} crystal; with specified Nd^{3+}-Nd^{3+} and Nd^{3+}- O^{2-} distances b.

The cell parameters are as follows a = 8.771 Å, b = 9.012 Å, c = 13.057 Å, ß = 89.58° with V = 1032.05 Å ^{3} and Z = 4. In Fig. 1b, a dodecahedron of the first coordination sphere with distance lengths between ions emphasis can be observed. It is clearly seen that the length of the Nd^{3+}-O^{2-} distance changes in the range of 2.28-2.50 Å while the distance between the neighboring Nd^{3+} ions is relatively large (5.19 - 6.62 Å).

The phase purity of the $La_{1-x}Nd_xP_5O_{14}$ nanocrystals was confirmed by the X-ray diffraction (XRD) measurements (Fig. 2a). All of the observed reflections correspond to the reference profile of a monoclinic NdP_5O_{14} phase with a space group P 1 21/c1 (ISCD 2035). From the Rietveld analysis, the average grain size of the $La_{1-x}Nd_xP_5O_{14}$ nanocrystals was determined to be 45 nm. This result was confirmed by transmission electron microscopy (TEM) images (Fig. 2b). More TEM images can be found in the Supporting Information. However it is important to mention that the resolution of the images was limited due to low stability of phosphates crystals under high voltage of the electron beam. One can see a number of agglomerates composed of nanocrystals due to ferroelasticity of the pentaphosphate crystals[3].

Figure 2. The X-ray diffraction patterns of the $La_{1-x}Nd_xP_5O_{14}$ nanocrystals - a; and transmission electron microscopy (TEM) image of NdP_5O_{14} nanocrystals - b.

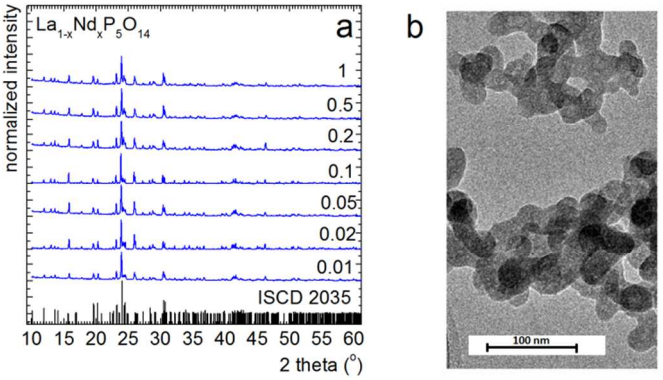

The back-scattering absorption spectra of the $La_{1-x}Nd_xP_5O_{14}$ nanocrystals are presented in Fig. 3. The spectra were normalized to the intensity of the $^4I_{9/2}\rightarrow{}^4F_{5/2}+{}^2H_{9/2}$ band. The most intense absorption bands are located at around 800 nm (see Fig. 3a), hence the 808 nm excitation line was chosen for photoluminescence measurements. It is worth mentioning that a significant impact of dopant ions on the absorption spectra can be observed. An increase of the dopant concentration entails the increase of the absorption band intensities in the UV-blue region. Especially it can be clearly observed for the $^4I_{9/2}\rightarrow{}^2D_{5/2}$ transition. The increase of the absorption transition with the concentration of the dopant ions is associated by an efficient cooperative interaction between Nd^{3+} ions[24].

One can notice a significant impact of dopant ions on absorption transition intensities can be observed (Fig. 3 b). An increase of dopant concentration entails the relative increase of absorption band intensities for three selected transitions (see

Fig. 3b). This plot reveals a linear increase of absorption transition intensities in a function of dopant concentration. The differences in slopes of those trends probably result from the different oscillator strengths of those transitions. The aforementioned behavior can be explained by a cooperative absorption associated with a high concentration of dopant ions, similar to that reported in previous work for $LiLa_{1-x}Nd_xP_4O_{12}$ nanocrystals[27].

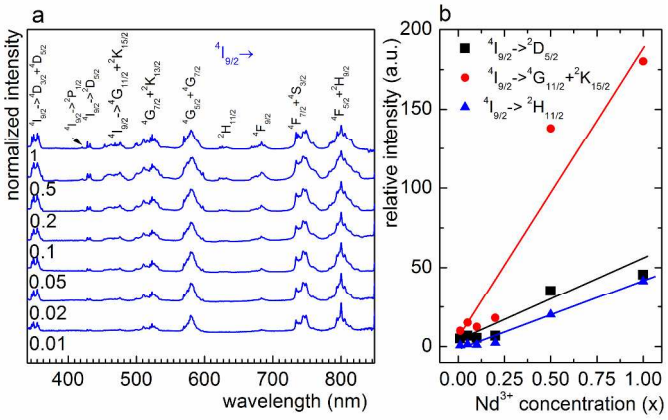

Figure 3. The back-scattering absorption spectra of LaP_5O_{14} nanocrystals-a; and the impact of the dopant concentration on the absorption transition intensities (intensities normalized to the intensity of the $^4I_{9/2}\rightarrow{}^2P_{1/2}$ transition).

For high dopant concentration, the population of the $^4I_{11/2}$ state becomes more efficient due to the $^4F_{3/2}\rightarrow{}^4I_{11/2}$ luminescence. After populating the $^4I_{11/2}$ state, the absorption both from $^4I_{9/2}$ and $^4I_{11/2}$ terms can occur leading to the cooperative absorption process. The intensity of the cooperative absorption transition I_{coop} is proportional to a square of the dopant concentration x so that the relative intensity of the absorption transitions shown in Fig. 3 b results in a linear plot $I_{coop}/I \sim x$, where I is the absorption intensity for non-interacting ions. The cooperative absorption transitions were reported previously for $LiLa_{1-x}Pr_xP_4O_{12}$ bulk crystals by Strek[32], for $PrCl_3$ crystals by Varsanyi and Dieke[33,34] and for Eu_2O_2S by Tanner and Pei[35]. A detailed discussion of the mechanism responsible for the cooperative absorption transitions in $LiLa_{1-x}Nd_xP_4O_{12}$ nanocrystals was recently presented by us[27].

The emission spectra of $La_{1-x}Nd_xP_5O_{14}$ nanocrystals were measured at room temperature using the 808 nm laser diode excitation line (see Fig. 4a). Three characteristic luminescence bands located at around 890 nm, 1060 nm and 1350 nm are associated with transitions from the excited $^4F_{3/2}$ state to the $^4I_{9/2}$, $^4I_{11/2}$ and $^4I_{13/2}$ multiplets. One can notice that in all presented spectra the so called 'laser transition' $^4F_{3/2}\rightarrow{}^4I_{11/2}$ is dominant. However with the increase of the dopant concentration the ratio of the transition intensities between particular bands changes. The emission branching ratio of the fluorescent transition intensities β_J from the $^4F_{3/2}$ state to the ^4I_J terminal states is

$$\beta_{J_1} = \frac{I_{J_1}}{\sum_{J=1}^{N} I_J} \qquad (1)$$

Where I_{J1} is the emission intensity of the $^4F_{3/2}\rightarrow{}^4I_{J1}$ transition and the sum in the denominator is taken over all the states into which a radiative depopulation of $^4F_{3/2}$ takes a place.

The effect of concentration on the intensity branching ratios is shown in Fig. 4b. One can see that the value of $\beta_{13/2}$ remains stable (~ 0.09) in the entire range of concentrations while $\beta_{9/2}$ as well as $\beta_{11/2}$ are strongly affected by the concentration. For the most diluted sample (x = 0.01) the band intensities are almost comparable ($\beta_{9/2}$=0.45 while $\beta_{11/2}$=0.55). However, with the increase of the Nd^{3+} concentration $\beta_{9/2}$ gradually decreases, while $\beta_{11/2}$ increases. The mechanism responsible for such behavior is associated with the fast diffusion of excitation energy corresponding to the resonant $^4F_{3/2}\rightarrow{}^4I_{9/2}$ transition. It is clearly seen (Fig. 4a) that with the increase of the dopant concentration the short wavelength part of the $^4F_{3/2}\rightarrow{}^4I_{9/2}$ transition band decreases. These components of the emission band are associated with the transition from $^4F_{3/2}$ to the Z_1 and Z_2 Stark levels of $^4I_{9/2}$. The energy diagram of Nd^{3+} ions in NdP_5O_{14} host is presented in fig. 5 with emphasize of two types of energy transfer which can takes place in this host. First of them is cross-relaxation $\{^4F_{3/2}, {}^4I_{9/2}\}\Leftrightarrow\{^4I_{15/2}, {}^4I_{15/2}\}$ (blue arrows) and fast energy diffusion between $^4F_{3/2}$ states (dark yellow arrows). Detailed analysis on probabilities of both of these processes will be given below.

According to the Judd-Ofelt theory[36,37] the transition probability of an electric dipole transition is given by

$$P^{ed}_{(S'L'J';SLJ)} = \frac{64\pi e^2}{3h(2J+1)}\lambda^{-3}\chi\sum_{t=2,4,6}\Omega_t\left|\left\langle SLJ\left\|U^t\right\|S'L'J'\right\rangle\right|^2 \qquad (2)$$

where e, h and λ are the elementary charge, the Planck constant and the emission wavelength, respectively. χ is the correction parameter depending on the refractive index n. Table 1 presents the $\left|\langle\|U^t\|\rangle\right|^2$ elements of the $^4F_{3/2}\rightarrow{}^4I_J$ transitions of Nd^{3+} and the Ω_t parameters of the NdP_5O_{14} matrix.

Table 1. The squared reduced-matrix elements $\left|\langle\|U^t\|\rangle\right|^2$ of the $^4F_{3/2}\rightarrow{}^4I_J$ transitions of Nd^{3+} and the Ω_t parameters of the NdP_5O_{14} matrix[38].

Transition	$\left\|\langle\|U^2\|\rangle\right\|^2$	$\left\|\langle\|U^4\|\rangle\right\|^2$	$\left\|\langle\|U^6\|\rangle\right\|^2$
$^4I_{15/2}$	0	0	0.0288
$^4I_{13/2}$	0	0	0.2085
$^4I_{11/2}$	0	0.1136	0.4104
$^4I_{9/2}$	0	0.2293	0.0548
	Ω_2 [10^{-20} cm^2]	Ω_4 [10^{-20} cm^2]	Ω_6 [10^{-20} cm^2]
NdP_5O_{14}	0.53	2.8	3.69

The fluorescent $^4F_{3/2}\rightarrow{}^4I_{15/2}$ transition was neglected due to a low probability related to a remarkably low value of $\left|\langle\|U^6\|\rangle\right|^2$.

The change of β_J is probably associated with the reabsorption process of the $^4F_{3/2} \rightarrow {}^4I_{9/2}$ emission for which the absorption cross-section is relatively high (see Fig.3). The confirmation of this explanation can also be found in the changes in the shape of the $^4F_{3/2} \rightarrow {}^4I_{9/2}$ transition within the entire range of Nd^{3+} concentrations. In the case of an insignificant contamination by an active ion, one can observe relatively intense lines around 863 nm and 870 nm related to the transitions from two Stark components ($^4F_{3/2} \rightarrow R_2$ and R_1, respectively) to the ground component of $^4I_{9/2}$ (Z_1). Nevertheless, with the increase of the number of active ions, a consistent decrease of the relative intensity of those two bands can be observed. Those bands correspond to the fundamental absorption to the first emitting state. Similar observation have been reported previously for so the called fully concentrated stoichiometric phosphors $LiNdP_4O_{12}$ [28].

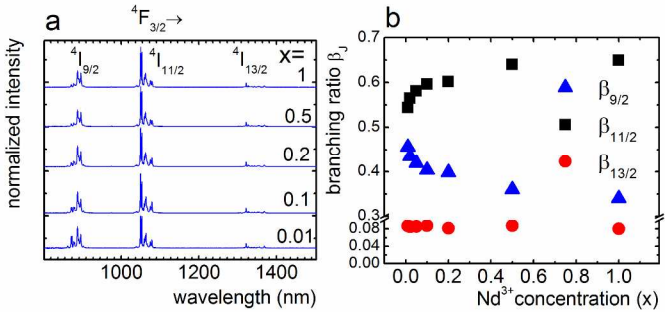

Figure 4. The luminescence spectra of $La_{1-x}Nd_xP_5O_{14}$ nanocrystals measured at 77K (a); the concentration dependence of the branching ratios β_J (b) and energy diagram of Nd^{3+} ions in NdP_5O_{14} nanocrystals (c).

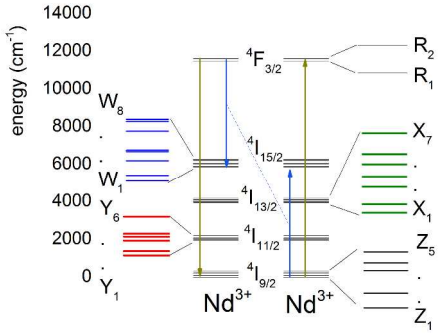

Figure 5. The energy diagram of Nd^{3+} ions in NdP_5O_{14} nanocrystals with marked cross-relaxation (blue arrows) and fast energy diffusion (dark yellow arrows) processes.

The kinetics of the $^4F_{3/2}$ multiplet has been studied as a function of the dopant concentration. From the decay curves presented in Fig. 6a one can notice that for low concentration of the Nd^{3+} ions the distance between them is sufficiently large to prevent the impact of ion-ion interactions so that exponential dependencies are observed.

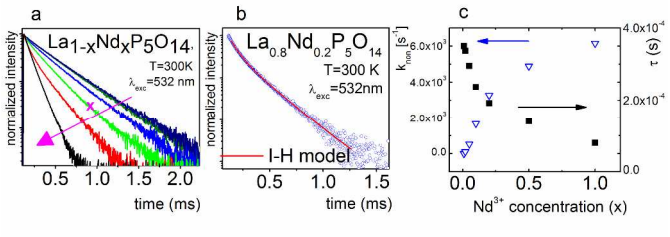

Figure 6. The $^4F_{3/2}$ luminescence intensity decays in $La_{1-x}Nd_x P_5O_{14}$ nanocrystals – (a);t he $^4F_{3/2}$ luminescence decay for $La_{0.8}Nd_{0.2}P_5O_{14}$ nanocrystals fitting using Inokuti-Hirayama model– (b); the $^4F_{3/2}$ luminescence decay rate and decay time as a function of the dopant concentration – (c)

For the Nd^{3+} concentration above x = 0.1, the luminescence decay profiles reveal a nonexponential shape due to the cooperative donor-acceptor interactions. However, for the higher concentration, the decay exhibits an exponential profile due to the energy diffusion process through the Nd^{3+} sublattice. The donor-donor interaction between the excited Nd^{3+} ions is responsible for the excited state energy migration (diffusion). In the case of coexistence of the donor-acceptor and donor-donor interactions, the fluorescence decay kinetics may be described by the Yokota-Tanimoto model[39]. The temporal evolution of the intensity can be expressed as follows

$$I(t) = I_0\left[\exp\left(-\frac{t}{\tau_0}\right) - \alpha\left(\frac{t}{\tau_0}\right)^{3/S} \times \left(\frac{1+10.866Z+15.50Z^2}{1+8.749Z}\right)^{(S-3)/(S-2)}\right] + b \quad (3)$$

where

$$\alpha = \frac{4}{3}\pi\Gamma\left(1-\frac{3}{s}\right)N_D R_0^3 \quad (4)$$

and

$$Z = DC_{DD}^{-2/S} t^{1-2/S} \quad (5)$$

Here S defines the character of the ion-ion interaction (S = 6, 8, 10 for the dipole-dipole, dipole-quadrupole, and quadrupole-quadrupole interactions, respectively), τ_0 is the radiative life time (for $La_{1-x}Nd_xP_5O_{14}$, the value of τ_0=330 μs was adopted), N_D is the dopant concentration (for NdP_5O_{14}, $N_D = 4 \cdot 10^{21}$ ions/cm^3), $\Gamma$is Euler gamma function, I_0 is the initial intensity and b is the fitting offset. The numerical coefficients preceding Z are the Padee parameters derived for the dipole-dipole interaction. D and C_{DD} – are the diffusion rate and the donor-donor interaction constant, respectively. The critical distance R_0 can be recast as

$$R_0 = \sqrt[3]{\frac{\alpha}{\frac{4}{3}\pi\Gamma\left(1-\frac{3}{s}\right)N_A}} \quad (6)$$

The most accurate approximation presented in Fig. 6b was obtained for the S = 6 value which points to the dipole-dipole interaction. Using R_0, the donor-acceptor interaction parameter C_{DA} is given by

$$C_{DA} = R_0^6 \cdot \tau_0 \quad (7)$$

A magnitude of the donor–acceptor interaction parameter C_{DA} may be obtained from fitting the emission decay profiles of $La_{0.8}Nd_{0.2}P_5O_{14}$ for which the fast diffusion is negligible. In such a case, the kinetics of the fluorescence intensity may described within the Inokuti-Hirayama model[40] as

$$I(t) = I_0\left[\exp\left(-\frac{t}{\tau_0}\right) - \alpha\left(\frac{t}{\tau_0}\right)^{3/S}\right] + b \quad (8)$$

Hence, the value of $C_{DA}=3.46\cdot10^{-44}$ m^6/s, which can be used to determine the donor-donor interaction parameter C_{DD} by fitting the luminescence decay profile of NdP_5O_{14}. $C_{DD}=4.7\cdot10^{-44}$ m^6/s and is one order of magnitude greater than C_{DA} confirming dominance of a fast energy diffusion over the donor-acceptor interaction responsible for the cross-relaxation transfers. The luminescence decay constant of the nanocrystalline stoichiometric phosphor NdP_5O_{14} was found to be around 90 µs and is was much smaller in comparison with one obtained by Huber for single crystal[41]. However the decay time for single crystal reported by Danielmeyer et al.[14] was much shorter (~ 60 µs) than the one reported by us in nanocrystals. Those differences may be caused by the quality of crystals.

The diffusion rate should be temperature dependent therefore the decay time measurements as a function of temperature have been performed for the NdP_5O_{14} nanocrystals (Fig. 7a). One can distinguish three parts of the presented dependence. In the 10 - 80 K temperature range (part A), an increase of temperature leads to a decrease of the decay constant due to the phonon-assisted depopulation of the $^4F_{3/2}$ multiplet. However, above 80 K, the decay time starts to increase with temperature up to 200 K (part B) and above that again exhibits slight decrease. In order to explain this behavior, a comparison of the 10 K and 100 K emission spectra with the room temperature absorption spectra is presented in Fig. 7b.

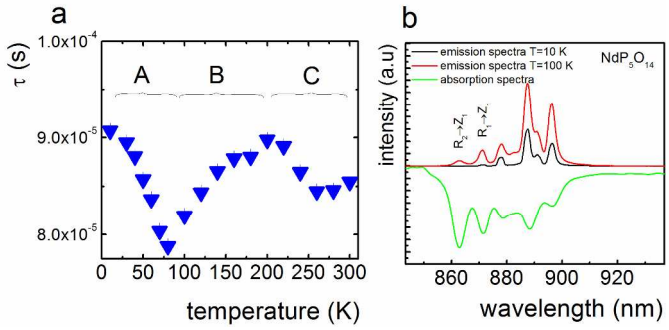

Figure 7. Temperature dependence of the decay time for the NdP_5O_{14} nanocrystals (a); and comparison of 10K, 100K emission spectra with 300K absorption spectra of NdP_5O_{14} (b).

The spectra have been limited only to the resonant $^4F_{3/2}\rightarrow{}^4I_{9/2}$ transition. The energy difference between the two Stark components R_1 and R_2 of the excited $^4F_{3/2}$ multiplet in the NdP_5O_{14} lattice is about 110 cm^{-1}. Therefore, above 80 K ($k_BT \approx 55cm^{-1}$) a population of the R_2 state becomes significant and emission from this state – possible. In the 10 K emission spectra (black line) only a transition from the R_1 state can be observed while emission from R_2 is absent. However, in the 100 K emission spectra (red line), an increase of the relative intensity from R_2 can be observed (especially for $R_2 \rightarrow Z_1$ at about 863 nm). On the other hand, the highest absorption cross-section can be observed precisely for the $Z_1\rightarrow R_2$ transition. Hence, one can conclude that for temperatures above 80 K, a fast diffusion is much more probable due to the energy resonance having an impact on the increase of the decay constant. However, above 200 K the lifetime decreases slightly again. At 200 K ($k_BT \approx 150$ cm^{-1}) – the thermal energy is sufficient for bridging the cross-relaxation transition [R_2(11583cm^{-1}), Z_1(0cm^{-1}))+$\hbar\omega$(150cm^{-1})⇔(W_1(5872cm^{-1}), W_1(5872cm^{-1})]. For the $La_{1-x}Nd_xP_5O_{14}$ nanocrystals, the cross-relaxation is strongly reduced and the energy migration process becomes dominant.

Conclusions

The novel method of $La_{1-x}Nd_xP_5O_{14}$ nanocrystals synthesis was described. The average grain sizes were determined to be 45 nm using Rietveld analysis and transmission electron microscopy. The impact of Nd^{3+} concentration on the spectroscopic properties of the $La_{1-x}Nd_xP_5O_{14}$ nanocrystals have been investigated. It was found that the Nd^{3+} concentration strongly affects the intensities of the absorption transitions, whereby intense cooperative absorption transitions were observed. The distribution of emission intensities of particular $^4F_{3/2}\rightarrow{}^4I_J$ transitions is strongly affected by the concentration of the Nd^{3+} ions. It was shown that $\beta_{9/2}$ decreases from 0.45 to 0.35 whereas $\beta_{11/2}$ demonstrated quite an opposite behavior and increases from 0.55 to 0.65. It was concluded that a reabsorption process is responsible for this behavior. Following the Judd-Ofelt theory the calculation of the emission branching ratios of fluorescence intensities β_J from $^4F_{3/2}$ to ^4I_J was performed. In particular, the process of concentration quenching of the Nd^{3+} fluorescence was investigated. It was found that the concentration quenching in the $La_{1-x}Nd_xP_5O_{14}$ nanocrystals is strongly reduced due to the relatively large distance between the neighboring Nd^{3+} ions in this host. The kinetics of the Nd^{3+} fluorescence was measured and discussed in terms of the Yokota-Tanimoto model. It was observed that the role of the donor-acceptor interaction responsible for the cross-relaxation is significant and leads to a nonexponential fluorescence decay dependencies in the intermediate concentration range $0.1 < x < 0.9$. For a fully concentrated crystal NdP_5O_{14}, corresponding to $x = 1$, the decay profiles became exponential again due to the large donor-donor interaction responsible for energy migration that prevails the donor-acceptor interaction between the Nd^{3+} ions.

Acknowledgements

L. M. acknowledges support from the NCN under grant no. 2012/05/N/ST5/02327. Authors would like to acknowledge dr Yuri Strzhemechny for critical reading of this manuscript.

Notes and references

[a] Institute of Low Temperature and Structure Research, Polish Academy of Sciences, Wroclaw, Poland
[b] Institute Light & Matter , Claude Bernard Lyon 1 University, UMR5306 CNRS, 69622 Villeurbanne, France
*corresponding author email: l.marciniak@int.pan.wroc.pl
Electronic Supplementary Information (ESI) available: [details of any supplementary information available should be included here]. See DOI: 10.1039/b000000x/

1 G. Winzer, P. G. Möckel, R.Oberbacher, L. Vité, Appl Phys 1976, **11**, 121.
2 S. R. Chinn, W. K. Zwicker, S. Colak, *J. Appl. Phys.* 1982, **53**, 5471.
3 G. M. Loiacono, M. Delfino, W. A. Smith, Appl. Phys. Lett. 1978, 32, 595.
4 C. Barthou, B. Blanzat, J. M. Létoffé, *J. Appl. Phys.* 1981, **52**, 6847.
5 H. P. Weber, *Opt Quant Electron* 1975, **7**, 431.
6 W. Strek, C. Szafrański, E. Łukowiak, Z. Mazurak, B. Jeżowska-Trzebiatowska, *Physica Status Solidi (a)* 1977, **41**, 547.
7 J. B. Gruber, D. K. Sardar, T. H. Allik, B. Zandi, *Opt Mater* 2004, **27**, 351.
8 I. Ismailov, B. Khalikov, *Sov. J. Quantum Electron* 1978, **8**, 537.
9 M. Szymański, J. Karolczak, F. Kaczmarek, *Appl. Phys* 1979, **19**, 345.
10 M. I. Gaiduk, V. V. Grigoryants, M. E. Zhabotinskii, A. A. Makovetskii, R. P. Tishchenko, *Sov. J. Quantum Electron.* 1979, **9**, 250.
11 X. R. Huang, Z. W. Hu, S. S. Jiang, J. H. Jiang, Y. L. Tian, Y. Han, J. Y. Wang, *J. Appl. Phys.* 1994, **75**, 7756
12 G. Huber, W. W. Krühler, W. Bludau, H. G. Danielmeyer, *J. Appl. Phys.* 1975, **46**, 3580.
13 J. B. Gruber, D. K. Sardar, T. H. Allik, B. Zandi, *Opt Mater* 2004, **27**, 351.
14 G. Danielmeyer, H. P. Weber, *IEEE J.Quant. Electron.* 1972, **QE-8**, 805.
15 K. Hickmann, V. John, A. Oertel, K. Koempe, M. Haase, *J Phys Chem C* 2009, **113** 4763.
16 P. Godlewska, S. Bandrowski, L. Macalik, R. Lisiecki, W. Ryba-Romanowski, I. Szczygieł, I. P. Ropuszyńska-Robak, J. Hanuza, *Opt Mater* 2012, **34**, 1023.
17. G. Zhang, Q. Zhang, Y. L. Shen, Q. L. Zhou, L. L. Hu, J. R. Qiu, D. P. Chen, *Laser Phys* 2011, **21**, 410.
18. A. J. Cramer, J. M. Cole, V. Fitzgerald, V. Honkimaki, M. A. Roberts, T. Brennan, R. A. Martin, G. A. Saunders, R. J. Newport, *PCCP* 2013, **15**, 8529.
19 Y. Wang, J. Li, J. Wang, S. Han, Y. Guo, *J Cryst Growth*, 2010, **312**, 2779.
20 D. Petrov, B. Angelov, V. Lovchinov, *J Rare Earth*, 2013, **31**, 485.
21 E. Suljoti, M. Nagasono, A. Pietzsch, K. Hickmann, D. M. Trots, M. Haase, W. Wurth, A. Föhlisch, *J Chem Phys* 2008, **128**, 134706
22 Y.-P. Fang, A.-W. Xu, R.-Q. Song, H.-X. Zhang, L.-P. You, J.C. Yu, H.-Q. Liu, *J Am Chem Soc*, 2003, **125**, 16025.
23 L. Marciniak, D. Hreniak, W. Strek J. Mater. Chem. C, 2014 DOI: 10.1039/C4TC00682H
24 L. Marciniak, W. Strek, A. Bednarkiewicz, A. Lukowiak, D. Hreniak, *Opt. Mater.* 2011, **33**, 1492
25 W. Strek, L. Marciniak, A. Bednarkiewicz, A. Lukowiak, D. Hreniak, R. Wiglusz, *Opt Mat* 2010, **33**, 1097.
26 W. Strek, L. Marciniak; A. Lukowiak, A. Bednarkiewicz, D. Hreniak, *Opt Mat* 2010, **33**, 131.
27 L. Marciniak, W. Strek, D. Hreniak, *Chem Phys Lett*, 2013, **583**, 151.
28 L. Marciniak, W. Strek, D. Hreniak, *J Lumin.* 2014, **148**, 214.
29 H. Y. P. Hong, *Acta Cyst,* 1974, **B30**, 468.
30 S. Jaulmes, *C. R. Acad Sci Paris, Sdr. C*, 1969, **268**, 935.
31 M. Beucher, *Les Elements des Terres Rares, Coll.* No. 1970, **180**, 331.
32 W. Strek, C. Szafranski, B. Jezowska-Trzebiatowska, *Acta Phys. Pol.* 1981, **A60**, 477.
33 F. Varsanyi, G. H. Dieke, *Phys. Rev. Lett*, 1961, **7**, 442
34 K. Shinagawa, *J. Phys. Soc. Jpn*, 1967, **23**, 1057.
35 P. A. Tanner, Z.-W. Pei, *J. Phys. Chem. Solids* 2001, **62**, 683.
36 B. R. Judd, *Phys. Rev.*, 1962, **127**, 750.
37 G. S. Ofelt, *J. Chem. Phys.*, 1962, **37**, 511.
38 A. Kaminskii, Crystalline Lasers: Physical Processes and Operating Schemes, CRC Press; 1996
39 T. Yokota, O. Tanimoto, *J. Phys. Soc. Japan* 1967, **22**, 779.
40 M. Inokuti; F. Hirayama, *J. Chem. Phys*. 1965, **43**, 1978.
41 G. Huber, H. G. Danielmeyer, *Appl Phys* 1979, **18**, 77.

